atmosphere

Article

Future Climate Prediction Based on Support Vector Machine Optimization in Tianjin, China

Yang Wang [1,*], Xijun Wang [1], Xiaoling Li [1], Wei Liu [1] and Yi Yang [2]

[1] Information Management Department, Northwest A&F University, Xianyang 712100, China
[2] School of Civil Engineering, Xijing University, Xi'an 710000, China
* Correspondence: 1527wangyang@nwafu.edu.cn; Tel.: +86-18991291675

Abstract: Climate is closely related to human life, food security and ecosystems. Forecasting future climate provides important information for agricultural production, water resources management and so on. In this paper, historical climate data from 1962–2001 was used at three sites in Tianjin Baodi, Tianjin and Tanggu districts as baseline and the model parameters were calibrated by the Long Ashton Research Station Weather Generator (LARS-WG). 2m-temperatures in 2011–2020 were verified under two scenarios, representative concentration pathway (RCP) 4.5 and RCP8.5 in different atmospheric circulation models with optimal minimum 2m-temperatures at the three sites. From 2031–2050, Tianjin will be using more moderate minimum 2m-temperatures in future simulations. Support vector machines (SVM) were used to optimize the simulated data to obtain more accurate future maximum and minimum 2m-temperatures for the three sites. The results showed that the determinant coefficient of LARS-WG simulation was 0.8 and SVM optimized determinant coefficient was 0.9 which greatly improved the prediction accuracy. The minimum and maximum future 2m-temperatures optimized under European Community Earth System Model (EC-EARTH) were relatively low and the same future 2m-temperatures optimized under Hadley Centre Global Environment Model Earth System (Had-GEM2-ES4) were high especially in the RCP8.5 scenario which simulated 2051–2070 climate. The SVM optimization showed that the maximum and minimum 2m-temperatures were in general agreement with the original simulation values.

Keywords: atmospheric general circulation model; future climate; LARS-WG; maximum 2m-temperature; minimum 2m-temperature; SVM optimization

Citation: Wang, Y.; Wang, X.; Li, X.; Liu, W.; Yang, Y. Future Climate Prediction Based on Support Vector Machine Optimization in Tianjin, China. *Atmosphere* **2023**, *14*, 1235. https://doi.org/10.3390/atmos14081235

Academic Editor: Jens Hesselbjerg Christensen

Received: 15 June 2023
Revised: 27 July 2023
Accepted: 28 July 2023
Published: 31 July 2023

1. Introduction

During the last century, the global climate has been warmed significantly with the average surface 2m-temperature increasing by about 0.9 °C between 1900 and 2018 [1]. In the 21st century, the 2m-temperature will rise further according to the four representative concentration path scenarios. Projected 2m-temperature increases by the end of the century are 0.30 °C–1.70 °C under the RCP2.6 scenario, 1.10 °C–2.60 °C under the RCP4.5 scenario, 1.40 °C–3.10 °C under the RCP6.0 scenario, and a projected increase of 2.60 °C–4.80 °C under the RCP8.5 scenario [2]. This global warming is mainly attributed to the increase in greenhouse gases, especially nitrous oxide, carbon dioxide, and ozone [3]. Changes in the global average 2m-temperature disrupt the environment, agriculture, food security, human health, and ecosystems [4]. In recent years, climate anomalies have seriously affected haze variability in North China [5] and extreme weather events occur frequently in China. Extreme heat events occurring during the flowering-sensitive stage of crop development can also significantly reduce grain yield, while sustained extreme heat may lead to almost total grain loss [6].

Meteorological elements are closely related to human life and the accurate prediction of meteorological elements provides important information for urban planning, land use, civil engineering design, and water resources management [7]. Meteorological data were applied to different general atmospheric circulation models (e.g., CanESM2, BCC-CSM1-1, and MICROC5) to simulate precipitation and the 2m-temperature under representative concentration path scenarios RCP4.5 and RCP8.5. Global climate models (GCM) simulate global climate based on possible future greenhouse gas scenarios. The current horizontal resolution of GCM is about 150 km and the spatial resolution of GCM varies [8]. Due to the lack of fine spatial resolution of the output of GCM, it is generally not used directly, but downscaling techniques are used for simulation prediction.

A stochastic weather generator is a probabilistic model that simulates the future climate of a specific location by analyzing historical climate data and then generates weather variables with the same statistical properties as historical data [9]. Daily weather data generated by these models have been used in various climate change studies in agriculture and hydrology [10,11]. LARS-WG is a well-known statistical downscaling model often used in climate prediction by constructing a climate change prediction model based on the vector autoregression (VAR) model and considering the impact of historical meteorological data on future climate for downscaling GCM outputs, such as 2m-temperature, precipitation, and solar radiation. For example, LARS-WG is used to simulate the 2m-temperature and precipitation in two RCP-(4.5 and 8.5) scenarios of Coupled Model Intercomparison and Intervention Project Phase 5 (CMIP5) [4]. LARS-WG combined with the genetic programming method was used to predict the future climate change of the Sanjabi Basin in Iran; the 2m-temperature and rainfall in the fifth Intergovernmental Panel on Climate Change (IPCC) report had been downscaled in comparison [12] to the simulated effects of climate change on maize yield under the Rcp scenario in Qazvin Plain, Iran [13]. There is literature [14] that uses LARS-WG to predict minimum 2m-temperature (Tmin), maximum 2m-temperature (Tmax), and precipitation (P) values of future periods (2021–2040, 2041–2060, 2061–2080, and 2081–2100) under RCP2.6, RCP4.5, and RCP8.5 scenarios. Driven by long-term (30 years) daily meteorological data, crop growth simulation models can be used to predict the impact of climate risks on crop growth and yield. However, the existence, availability, access, or required costs of high-quality, long-term daily weather data often severely constrain the use of crop models. In this case, the use of random weather generators can help overcome this limitation [15].

There are many studies using LARS-WG to predict future climate [16,17], and the accuracy of the LARS-WG prediction is higher than that of weather prediction models in simulating the future climate in Canadian regions [18]. Using the LARS-WG method, a 250-year meteorological series ensemble is synthesized from the observed historical series, and hydrological forecasts are made [19]. LARS-WG has been used to modeling future climate change in Texas using for an early response to frequent extreme weather events [20]. In recent years, machine learning algorithms have been used more and more widely and with better results. A neural network model was used to predict the future climate of the Iranian Caspian Sea for the next 20 years under the RCP4.5 and RCP8.5 emission scenarios with more simulation accuracy [21]. LARS-WG was utilized to predict future (2015–2044) climate variables in central Iran, and an artificial neural network was used to establish the relationship between climate variables and snow water equivalents during the baseline period to predict future snow water equivalents [22]. Future climate was simulated using LARS-WG for GCM output downscaling in the CMIP5 model, and three data mining models, namely the artificial neural network, support vector machine, and genetic expression programming, were used to predict runoff in future climate scenarios, and SVM simulation was found to have the highest performance [23].

Most of the above studies used LARS-WG to make projections of the future climate, and then analyzed the various metrics under the projected future climate scenarios. Therefore it becomes important to improve the accuracy of the future climate. With the intensification of global climate change, Tianjin as a coastal city in eastern China is facing increasingly severe climate problems. In this study, the SVM optimization algorithm is used to enhance the accuracy of future climate prediction under two future RCP scenarios and evaluate the advantages and disadvantages of the two methods in regional climate change. The main points of the study include: (1) the historical climate data and geographical data of Tianjin were first collected and pre-processed. (2) the VAR model is used to construct the climate prediction model of the LARS-WG method; and (3) the SVM method was used to train the model and then the trained model was used to optimize the prediction of the future climate.

2. Materials and Methods

2.1. Description of the Study Area

Tianjin is located in the northeast of China's North China Plain known as the "river and sea". It is located at 117°10′ E and 39°10′ N. Tianjin is located in the lower reaches of the Haihe River and straddles both sides of the Haihe River. The average annual 2m-temperature is about 14 °C, It is the hottest in July, where the average monthly 2m-temperature is 28 °C. The highest 2m-temperature on record was 41.6 °C. January is the coldest with an average monthly 2m-temperature of −2 °C. Annual precipitation a Annual rainfall ranges from 500 to 700 mm. Table 1 provides an overview of the specifications for the three sites, which contain station, latitude (Lat), longitude (Long), elevation (Elev), Tmax, Tmin, and P.

Table 1. Specifications of meteorological stations.

Station	Lat.	Long.	Elev. (m)	Tmax (°C)	Tmin (°C)	P. (mm/year)
Baodi54525	39.73	117.28	4.7	40.8	−27.4	672.0
Tianjin54527	38.59	117.43	5.6	40.5	−22.9	635.72
Tanggu54623	39.06	117.10	3.3	40.9	−17.1	719.51

2.2. Meteorological Data

Observations of daily Tmax and Tmin from 1962 to 2020 at the three sites were obtained from the National Climate Center. Downscaling records based on GCM data and LARS-WG simulation calibration was applied at three different stations in Baodi, Tianjin, and Tanggu. The Tmax and Tmin for 40 years from 1962 to 2001 were used for the baseline period. The climate projections of the GCM under two RCP scenarios, 2031–2050 (1950s) and 2051–2070 (1970s) are analyzed using the calibration with data from 2002 to 2020. Eight GCM (ACC, BCC, CanESM, CMCC, CNRM, CSIRO, EC-EARTH, and HadGEM2-ES) modes of the CMIP5 model were selected for climate prediction analysis under two typical concentration path scenarios, RCP4.5 and RCP8.5, respectively, as shown in Table 2. Due to the fact that the selected GCM modes all contain RCP4.5 and RCP8.5 scenarios, only some modes contain RCP2.6. In order to facilitate scene prediction and comparison between different modes, this study only considered RCP4.5 and RCP8.5 scenarios, without considering RCP2.6 scenarios.

Table 2. Atmospheric circulation patterns in the LARS-WG model.

GCM	Development Institute	Country	RCP
ACCESS1-3	European Organization for the Exploitation of Meteorological Satellites	European	2.6, 4.5, 8.5
BCC-CSM1-1	Beijing Climate Center	China	4.5, 8.5
CanESM2	Canadian Centre for Climate Modelling and Analysis	Canada	2.6, 4.5, 8.5
CMCC-CM	China Meteorological Administration	China	4.5, 8.5
CNRM-CM5	National Meteorological Research Centre and European Centre for Research and Advanced Training in Scientific Computing	France	4.5, 8.5
CSIRO-MK36	Commonwealth Scientific and Industrial Research Organization	Australia	2.6, 4.5, 8.5
EC-EARTH	European Commission—Joint Research Centre	European	4.5, 8.5
Had-GEM2-ES	Hadley Centre Global Environment	England	2.6, 4.5, 8.5

2.3. Methods

2.3.1. LARS-WG Model Approach

The LARS-WG 6 version was used in this study. The LARS-WG simulation in this study consists of three steps, firstly, using 40 years of daily observed weather data for model calibration through SITE ANALYSIS, we analyze the daily observed weather data (Tmax and Tmin) to determine the model parameters, and based on this, generate 40 years of synthetic daily weather data. We used Q-test analysis to validate the LARS-WG model to confirm the model accuracy. Second, the monthly mean weather statistical indices are evaluated based on observations and simulations, and then the relative change factors of the monthly GCMs outputs are calculated. Third, the daily maximum and minimum 2m-temperatures are simulated for the next 20 years.

2.3.2. SVM

SVM was proposed by Vapnik et al. [24] in 1995 and has been one of the most influential machine learning algorithms for over 20 years. SVM can not only be used for classification problems, but also for regression problems, such as time series analysis and pattern recognition problems, and can be extended to prediction and comprehensive analysis and other fields. Based on statistical learning theory, a classifier is established to predict future climate change. In regression problems, training samples are given first, and through learning the linear model hopes to make each sampling point as close to the shape as possible. To make $f(x)$ and y as close as possible, as shown in Equations (1) and (2),we use:

$$D = \{(x_1, y_1), (x_2, y_2), \ldots, (x_m, y_m)\}, y_i \in R, x_i \in R \tag{1}$$

$$f(x) = w^T x + b(w \in R, b \in R) \tag{2}$$

where x is the input vector, called the influence factor, y is the predicted object, and w and b are the model parameters to be determined.

Assuming a maximum error Δ is allowed between $f(x)$ and y, and the loss is only calculated when the absolute value of the difference between $f(x)$ and y is greater than Δ. We constructed an interval band with a width of 2Δ centered on $f(x)$. If the training sample falls into this interval band, the prediction is considered correct. Therefore, the SVR problem can be formalized as an equation:

$$\min_{w,b} \frac{\| w \|^2}{2} + C\sum_{i=1}^{m} l_\Delta(f(x_i) - y_i) \tag{3}$$

where C is the regularization constant and l_Δ is the loss function.

2.4. Statistical Evaluation Criterions

The Tmin and Tmax data of 40 years from 1962 to 2001 were collected and divided into a training set and a test set according to the ratio of 9:1. Two indexes, the coefficient of determination (R^2) and root mean square error (RMSE) were proposed to evaluate the performance of the prediction model. The coefficient of determination is mainly used to measure the correlation between actual and predicted values. The closer its value is to 1, the better the correlation between actual and predicted values. The calculation formula is as follows:

$$R^2 = 1 - \left[\frac{\sum_{i=1}^{N} (O_i - P_i)^2}{\sum_{i=1}^{N} (O_i - \bar{O}_i)^2} \right] \tag{4}$$

where O_i denotes the observed value, P_i denotes the simulated value, $\bar{O}$ denotes the average of the observed values, and N denotes the number of samples.

RMSE is mainly used to measure the deviation degree between the real value and the predicted value [25], and its calculation formula is as follows:

$$RMSE = \sqrt{\frac{\sum_{i=1}^{N} (O_i - P_i)^2}{N}} \quad (5)$$

3. Results and Discussions

3.1. LARS-WG

3.1.1. Baseline Data Comparison

LARS-WG was used to simulate the Tmax and Tmin from 1962 to 2001 in the baseline period. The results are shown in Figures 1–3. In the figure, the simulated values are denoted by "gen" and the observed values by "obs". It can be seen from Figure 1 that the simulated value of the lowest 2m-temperature in the Baodi district in March and May is slightly higher than the observed value, and the simulated value in June is slightly lower than the observed value; There is little difference between the simulated and observed results in the remaining months. The simulated value of the highest 2m-temperature in the Baodi district in March is slightly lower than the observed value, and the difference between the simulated and observed results in the remaining months is very small. Figure 2 shows that the simulated value of the lowest 2m-temperature in the Tianjin district in June is slightly lower than the observed value; and the simulated value in November is higher than the observed value and there is little difference between the simulated and observed results in the remaining months. There is a slightly larger difference between the observed and simulated value of the Tmin in Tianjin. The Tmin in the Tanggu district is slightly lower than the observed value in April, and there is little difference between the simulation and the observed value in other months. The Tmax in the Tanggu district is slightly lower than the observed value in February and April and there is little difference between the simulated and observed results in other months. From Figures 1–3, the lowest 2m-temperature occurs in January, which is about −11 °C in the Baodi district, −8 °C in the Tianjin district, and −6.5 °C in the Tanggu district. The highest 2m-temperature occurred in July, and the average Tmax at the three sites was around 30 °C. Tables 3–5 show the Kolmogorov-Smirnov (KS) test of Tmin and Tmax in the Baodi district, Tianjin district, and Tanggu district respectively. The effective number from January to December in the table is 11.5, and the p value is 1, indicating that the results are reliable.

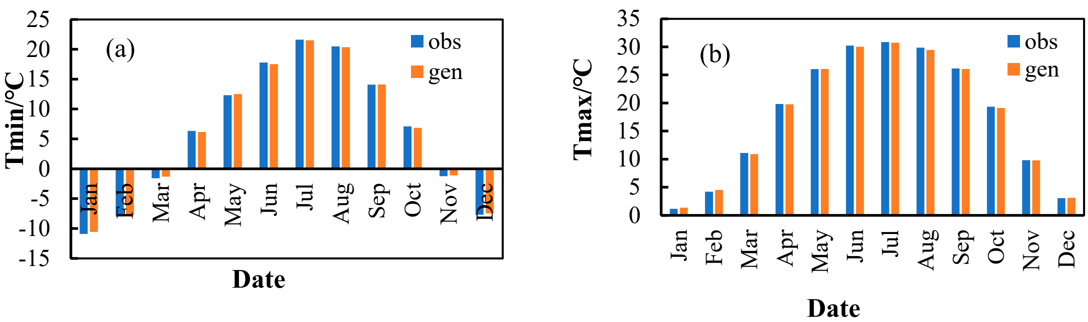

Figure 1. Observed and simulated values of (**a**) Tmin (**b**) Tmax in the Baodi district.

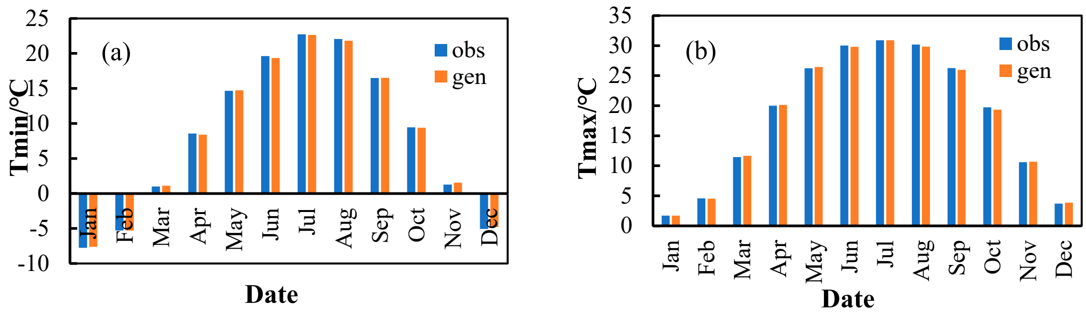

Figure 2. Observed and simulated values of (**a**) Tmin (**b**) Tmax in the Tianjin district.

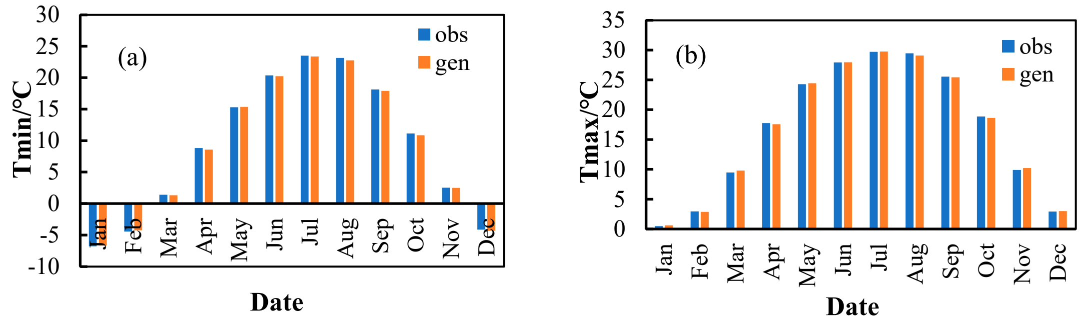

Figure 3. Observed and simulated values of (**a**) Tmin (**b**) Tmax in the Tanggu district.

Table 3. KS-test for Baodi daily Tmin and Tmax distributions.

KS-Test for Daily Tmin Distributions	Effective N	KS Statistic	*p*-Value	KS-Test for Daily Tmax Distributions	Effective N	KS Statistic	*p*-Value
J	11.5	0	1	J	11.5	0.052	1
F	11.5	0.053	1	F	11.5	0.052	1
M	11.5	0	1	M	11.5	0.053	1
A	11.5	0.053	1	A	11.5	0.053	1
M	11.5	0.053	1	M	11.5	0.053	1
J	11.5	0.053	1	J	11.5	0.053	1
J	11.5	0.053	1	J	11.5	0.053	1
A	11.5	0.053	1	A	11.5	0.106	0.999
S	11.5	0.053	1	S	11.5	0.053	1
O	11.5	0.053	1	O	11.5	0.053	1
N	11.5	0.052	1	N	11.5	0.053	1
D	11.5	0.033	1	D	11.5	0.053	1

Table 4. KS-test for Tanggu daily Tmin and Tmax distributions.

KS-Test for Daily Tmin Distributions	Effective N	KS Statistic	*p*-Value	KS-Test for Daily Tmax Distributions	Effective N	KS Statistic	*p*-Value
J	11.5	0.053	1	J	11.5	0.053	1
F	11.5	0.053	1	F	11.5	0.053	1
M	11.5	0.053	1	M	11.5	0.053	1
A	11.5	0.053	1	A	11.5	0.053	1
M	11.5	0.053	1	M	11.5	0.053	1
J	11.5	0.053	1	J	11.5	0.053	1
J	11.5	0.053	1	J	11.5	0.053	1
A	11.5	0.106	0.999	A	11.5	0.106	0.999
S	11.5	0.053	1	S	11.5	0.053	1
O	11.5	0.053	1	O	11.5	0.053	1
N	11.5	0.053	1	N	11.5	0.053	1
D	11.5	0.053	1	D	11.5	0.053	1

Table 5. KS-test for Tianjin daily Tmin and Tmax distributions.

KS-Test for Daily Tmin Distributions	Effective N	KS Statistic	*p*-Value	KS-Test for Daily Tmax Distributions	Effective N	KS Statistic	*p*-Value
J	11.5	0.033	1	J	11.5	0.053	1
F	11.5	0.053	1	F	11.5	0.053	1
M	11.5	0.053	1	M	11.5	0	1
A	11.5	0.053	1	A	11.5	0.053	1
M	11.5	0.052	1	M	11.5	0.052	1
J	11.5	0.106	0.999	J	11.5	0.053	1
J	11.5	0.053	1	J	11.5	0.053	1
A	11.5	0.106	0.999	A	11.5	0.106	0.999
S	11.5	0.053	1	S	11.5	0.105	0.999
O	11.5	0.053	1	O	11.5	0.053	1
N	11.5	0	1	N	11.5	0.053	1
D	11.5	0.01	1	D	11.5	0.053	1

In order to make the simulation results comparable, this study uses two scenarios of eight atmospheric circulation models in LARS-WG, RCP4.5 and RCP8.5 to simulate the 2011–2020 climate and compare them with the observed values. Table 6 shows the R^2 and RMSE of the model simulation. Table 6 shows that there is little difference in the simulation under the eight GCMs but the simulated Tmin determination coefficient is higher than the simulated Tmax determination coefficient. The R^2 of the highest 2m-temperature is around 0.8 and the R^2 of the lowest 2m-temperature is between 0.86 and 0.87 indicating that the lowest 2m-temperature by LARS-WG is better simulated. Therefore, it is more suitable to use LARS-WG to simulate the Tmin in Tianjin.

Table 6. Simulation accuracy under eight GCMs.

GCM	RCP	Baodi Tmax RMSE	R^2	Tmin RMSE	R^2	Tianjin Tmax RMSE	R^2	Tmin RMSE	R^2	Tanggu Tmax RMSE	R^2	Tmin RMSE	R^2
ACCESS1-3	RCP4.5	5.19	0.80	4.39	0.86	5.24	0.79	4.01	0.87	5.02	0.80	4.07	0.86
	RCP8.5	5.20	0.80	4.41	0.86	5.26	0.79	4.02	0.87	5.03	0.80	4.09	0.86
BCC-CSM1-1	RCP4.5	5.27	0.79	4.45	0.85	5.30	0.79	4.08	0.87	5.09	0.80	4.11	0.86
	RCP8.5	5.26	0.79	4.41	0.85	5.28	0.79	4.08	0.87	5.04	0.80	4.09	0.86
CanESM2	RCP4.5	5.30	0.79	4.49	0.85	5.32	0.78	4.10	0.87	5.12	0.79	4.17	0.86
	RCP8.5	5.26	0.79	4.40	0.85	5.27	0.79	4.08	0.87	5.05	0.80	4.11	0.86
CMCC-CM	RCP4.5	5.27	0.79	4.43	0.85	5.29	0.79	4.09	0.87	5.05	0.80	4.10	0.86
	RCP8.5	5.18	0.80	4.39	0.85	5.22	0.79	4.07	0.87	5.00	0.80	4.07	0.86
CNRM-CM5	RCP4.5	5.25	0.79	4.48	0.85	5.29	0.79	4.06	0.87	5.10	0.80	4.13	0.86
	RCP8.5	5.22	0.79	4.44	0.85	5.26	0.79	4.05	0.87	5.05	0.80	4.10	0.86
CSIRO-MK36	RCP4.5	5.22	0.80	4.44	0.85	5.26	0.79	4.04	0.87	5.03	0.80	4.07	0.86
	RCP8.5	5.21	0.80	4.40	0.84	5.27	0.79	4.05	0.87	5.05	0.80	4.07	0.86
EC-EARTH	RCP4.5	5.23	0.80	4.45	0.85	5.27	0.79	4.05	0.87	5.07	0.80	4.11	0.86
	RCP8.5	5.21	0.80	4.41	0.86	5.25	0.79	4.04	0.87	5.03	0.80	4.08	0.86
Had GEM2-ES	RCP4.5	5.21	0.80	4.41	0.86	5.22	0.79	4.08	0.87	4.98	0.80	4.06	0.86
	RCP8.5	5.21	0.80	4.41	0.86	5.22	0.79	4.12	0.87	5.01	0.80	4.08	0.86

3.1.2. Future Climate Projections

Four atmospheric circulation models, ACCESS1-3, CSIRO-MK36, EC-EARTH, and Had-GEM2-ES were selected. LARS-WG was used to simulate the Tmin and Tmax from 2031 to 2050s and 2051 to 2070s under two scenarios of RCP4.5 and RCP8.5 in the Baodi district, Tianjin district, and Tanggu district, and the results are shown in Tables 7–12. It can be seen from the tables that the lowest 2m-temperature occurred in January and the highest 2m-temperature occurred in July at the three sites, and the overall trend was consistent with the baseline period, but the 2m-temperatures were different in different scenarios. The Tmin and Tmax in the 1970s are both higher than in the 1950s, indicating that the future climate is a growing trend which is consistent with previous studies [26–28]. Among the four GCMs, the future Tmin and Tmax simulated by EC-EARTH are relatively low and the Tmin and Tmax simulated by Had-GEM2-ES4 are relatively high, especially in the RCP8.5 scenario, which simulates the future climate in the 2070s.

Table 7. Climate projections of Tmin for 2031–2050s and 2051–2070s in the two RCP scenarios under the four GCM models in Baodi (Note: ACCESS1-3, CSIRO-MK36, EC-EARTH, and Had-GEM2-ES are denoted by 1, 2, 3, and 4, respectively. The 50 represents the 2031–2050s and the 70 represents the 2051–2070s. The month is indicated by the first three letters).

	Jan	Feb	Mar	Apr	May	Jun	Jul	Aug	Sep	Oct	Nov	Dec
1-RCP45-50	−9.3	−6	0.5	7.4	13.9	19	22.9	21.9	15.7	8.1	−0.13	−6.4
1-RCP45-70	−8.2	−4.9	1.6	8.4	14.7	19.6	23.5	22.6	16.4	8.8	0.77	−5.3
1-RCP85-50	−8.9	−5.9	0.6	7.6	14.3	19.8	23.9	22.6	16.1	8.4	0.35	−5.7
1-RCP85-70	−6.9	−3.8	2.6	9.5	16.2	21.3	25.2	24	17.8	10.3	2.08	−4
2-RCP45-50	−8.5	−6.1	0.7	7.8	14	19	23.1	22.3	16.1	8.6	0.49	−5.2
2-RCP45-70	−7.7	−5.3	1.3	8.5	15.1	20.4	24.6	23.6	17.1	9.5	1.46	−4.4
2-RCP85-50	−8.5	−5.7	1	8	14.3	19.5	23.6	22.5	16.2	8.6	0.56	−5.4
2-RCP85-70	−6.9	−4.4	2	9	15.5	20.9	25.2	24.4	18	10.3	2	−3.8
3-RCP45-50	−9.7	−6.7	0.03	7.1	13.7	18.7	22.5	21.5	15.4	7.9	0.02	−6.2
3-RCP45-70	−9.2	−6.2	0.4	7.7	14.2	19.1	22.9	22.2	16.1	8.6	0.55	−5.8
3-RCP85-50	−9.5	−6.8	0.04	7.6	14.4	19.3	22.9	21.9	15.9	8.5	0.49	−5.9
3-RCP85-70	−8.3	−5.6	1.18	8.6	15.2	20.2	24.2	23.4	17.3	9.8	1.7	−4.7
4-RCP45-50	−8.2	−5.6	0.84	8.3	14.9	19.8	23.5	22.3	16.3	9.1	1.22	−5.1
4-RCP45-70	−7.4	−4.3	1.86	9.1	15.9	20.8	24.2	23.1	17.2	10	1.84	−4.8
4-RCP85-50	−8.1	−5.3	1.56	8.8	15.1	20	23.8	22.9	16.8	9.4	1.44	−4.7
4-RCP85-70	−5.4	−2.4	4.1	10.8	16.8	21.5	25.2	24.2	18.4	11.2	3.33	−2.4

Table 8. Climate projections of Tmax for 2031–2050s and 2051–2070s in the two RCP scenarios under the four GCM models in Baodi.

	Jan	Feb	Mar	Apr	May	Jun	Jul	Aug	Sep	Oct	Nov	Dec
1-RCP45-50	2.8	6.5	12.7	20.7	27.4	31.6	32.4	31	27.4	20.1	10.9	4.3
1-RCP45-70	3.9	7.6	13.8	21.8	28.1	32.2	33	31.7	28.1	20.8	11.8	5.4
1-RCP85-50	3.2	6.6	12.8	21	27.7	32.4	33.4	31.6	27.8	20.5	11.3	5
1-RCP85-70	5.2	8.7	14.8	22.9	29.6	34	34.7	33	29.6	22.4	13.1	6.6
2-RCP45-50	3.6	6.3	12.8	21.3	27.3	31.2	32.5	31.6	28.3	21.4	12.5	6
2-RCP45-70	4	6.7	13.4	22.3	28.7	33.1	34.7	33.4	29.6	22.9	13.9	6.8
2-RCP85-50	3.7	6.7	13	21.1	27.7	32	32.9	31.3	27.9	21.2	12.6	6
2-RCP85-70	4.9	7.7	14	22.4	28.8	33.2	34.9	34	30.6	23.6	14.4	7.4
3-RCP45-50	2.4	5.8	12.2	20.5	27.1	31.3	32	30.5	27.1	20	11	4.5
3-RCP45-70	3	6.2	12.6	21.1	27.7	31.6	32.5	31.2	27.8	20.7	11.6	4.9
3-RCP85-50	2.7	5.7	12.2	21	27.9	31.8	32.4	30.9	27.6	20.6	11.5	4.8
3-RCP85-70	3.9	6.9	13.3	22	28.6	32.8	33.7	32.4	29	21.9	12.7	6
4-RCP45-50	2.7	6.2	13.1	22.4	28.7	32.5	33.2	32.3	28.5	20.9	11.4	5
4-RCP45-70	4.7	8.7	14.7	23.3	29.9	33.6	33.5	32.4	29	21.5	12.3	6.3
4-RCP85-50	3.1	6.6	13.6	22.3	28.9	32.8	33.7	32.4	28.8	21.3	12	5.3
4-RCP85-70	5.7	9.2	16	23.9	30	34.1	34.9	33.6	30.4	22.8	13.4	7.4

Table 9. Climate projections of Tmin for 2031–2050s and 2051–2070s in the two RCP scenarios under the four GCM models in Tianjin.

	Jan	Feb	Mar	Apr	May	Jun	Jul	Aug	Sep	Oct	Nov	Dec
1-RCP45-50	−6.3	−3.45	2.63	9.77	16.23	21	24.2	23.35	17.94	10.69	2.41	−3.76
1-RCP45-70	−5.2	2.43	3.7	10.77	16.88	21.45	24.78	24.1	18.71	11.44	3.32	−2.66
1-RCP85-50	−6	−3.44	2.7	9.95	16.51	21.71	25.18	23.92	18.31	11.02	2.86	−3.13
1-RCP85-70	−4.1	−1.33	4.72	11.96	18.4	23.26	26.54	25.49	20.19	13	4.65	−1.52

Table 9. *Cont.*

	Jan	Feb	Mar	Apr	May	Jun	Jul	Aug	Sep	Oct	Nov	Dec
2-RCP45-50	−5.6	−3.37	2.82	10.08	16.2	20.8	24.22	23.65	18.44	11.26	3.02	−2.79
2-RCP45-70	−4.8	−2.58	3.58	10.91	17.3	22.23	25.80	24.9	19.41	12.26	4.05	−1.96
2-RCP85-50	−5.5	−2.94	3.19	10.33	16.62	21.42	24.77	23.84	18.5	11.37	3.15	−2.86
2-RCP85-70	−4	−1.62	4.29	11.38	17.78	22.71	26.38	23.74	20.31	13.01	4.58	−1.38
3-RCP45-50	−6.6	−4.03	2.34	9.53	15.93	20.61	23.77	22.97	17.72	10.61	2.60	−3.56
3-RCP45-70	−6.1	−3.53	2.68	10.07	16.42	20.91	24.22	23.68	18.43	11.29	3.14	−3.14
3-RCP85-50	−6.4	4.05	2.23	9.90	16.51	21	23.98	23.24	18.2	11.19	3.05	−3.24
3-RCP85-70	−5.2	−2.56	3.39	10.89	17.33	21.96	25.28	24.7	19.58	12.44	4.21	−2.09
4-RCP45-50	−5.7	−3.4	2.97	10.47	16.72	21.2	24.39	23.62	18.39	11.29	3.30	−2.64
4-RCP45-70	−5	−2.17	4.02	11.36	17.79	22.24	25.17	24.37	19.35	12.23	3.92	−2.30
4-RCP85-50	−5.3	−2.77	3.54	10.84	17.01	21.53	24.74	24	18.88	11.85	3.77	−2.34
4-RCP85-70	−2.5	0.16	6.06	12.84	18.72	23.11	26.18	25.41	20.55	13.7	5.71	0.01

Table 10. Climate projections of Tmax for 2031–2050s and 2051–2070s in the two RCP scenarios under the four GCM models in Tianjin.

	Jan	Feb	Mar	Apr	May	Jun	Jul	Aug	Sep	Oct	Nov	Dec
1-RCP45-50	3.1	6.57	13.24	21.47	27.77	31.15	32.69	31.44	27.42	20.71	11.53	4.88
1-RCP45-70	4.2	7.6	14.31	22.51	28.40	31.56	33.22	32.18	28.21	21.44	12.44	5.98
1-RCP85-50	3.4	6.58	13.31	21.66	28	31.87	33.62	32	27.78	21.03	11.97	5.5
1-RCP85-70	5.3	8.69	15.32	23.68	29.92	33.42	34.9	33.57	29.69	23.05	13.78	7.13
2-RCP45-50	3.9	6.47	13.41	21.98	27.77	30.74	32.62	31.97	28.36	21.99	13.12	6.51
2-RCP45-70	4.3	6.87	14.01	22.98	29.12	32.68	34.87	33.7	29.73	23.56	14.57	7.31
2-RCP85-50	4.1	6.99	13.64	21.83	28.13	31.59	33.02	31.73	28.09	21.97	13.32	6.62
2-RCP85-70	5.1	7.90	14.70	23.11	29.15	32.69	35.02	34.37	30.69	24.23	14.99	7.86
3-RCP45-50	2.8	5.98	12.85	21.26	27.48	30.75	32.21	31.05	27.22	20.61	11.75	5.07
3-RCP45-70	3.3	6.48	13.28	21.82	27.98	31.01	32.66	31.76	27.93	21.31	12.29	5.5
3-RCP85-50	3	5.96	12.81	21.64	28.11	31.14	32.42	31.32	27.7	21.23	12.20	3.38
3-RCP85-70	4.2	7.15	13.98	22.64	28.88	32.08	33.72	32.78	29.09	22.46	13.35	6.53
4-RCP45-50	3.6	6.78	14.11	22.92	29.03	32.02	33.46	32.45	28.56	21.5	12.25	5.74
4-RCP45-70	5.6	9.33	15.94	23.97	30.3	33.16	33.79	32.59	29.07	22.23	13.30	7.19
4-RCP85-50	3.7	7.2	14.55	23.17	30.15	32.14	33.72	32.67	28.73	21.81	12.63	5.96
4-RCP85-70	6.5	9.99	16.94	24.81	30.49	33.65	35.03	34.04	30.48	23.48	14.16	8.19

Table 11. Climate projections of Tmin for 2031–2050s and 2051–2070s in the two RCP scenarios under the four GCM models in Tanggu.

	Jan	Feb	Mar	Apr	May	Jun	Jul	Aug	Sep	Oct	Nov	Dec
1-RCP45-50	−5.15	−2.39	3.04	9.97	16.6	21.77	25	24.46	19.54	12.08	3.64	−3.36
1-RCP45-70	−4.07	−1.4	4.1	10.97	17.25	22.23	25.58	25.28	20.36	12.85	4.57	−2.23
1-RCP85-50	−4.81	−2.41	3.11	10.15	16.86	22.47	25.95	25.06	19.91	12.39	4.09	−2.73
1-RCP85-70	−2.97	−1.33	5.14	12.16	18.72	23.98	27.3	26.69	21.8	14.45	5.92	−1.12
2-RCP45-50	−4.38	−2.18	3.24	10.21	16.54	21.51	24.83	24.65	19.98	12.63	4.24	−2.46
2-RCP45-70	−3.64	−1.37	4.07	11.10	17.68	22.96	26.43	25.90	20.97	13.66	5.33	−1.61
2-RCP85-50	−4.35	−1.79	3.6	10.49	17.03	22.19	25.42	24.85	20.06	12.78	4.42	−2.51
2-RCP85-70	−2.80	−0.42	4.77	11.60	18.17	23.43	26.99	26.73	21.85	14.41	5.85	−1.03
3-RCP45-50	−5.37	−2.88	2.7	9.75	16.30	21.34	24.48	24.09	19.33	11.95	3.80	−3.11
3-RCP45-70	−4.84	−2.36	3.16	10.27	16.75	21.65	24.92	24.75	19.99	12.60	4.31	−2.71
3-RCP85-50	−5.12	−2.82	2.73	10.06	16.79	21.64	24.57	24.23	19.71	12.47	4.21	−2.81
3-RCP85-70	−3.97	−1.66	3.86	11.03	17.56	22.55	25.81	25.66	21.08	13.69	5.33	−1.69
4-RCP45-50	−4.42	−2.16	3.45	10.65	17.07	21.96	25.11	24.74	20.05	12.73	4.57	−2.18
4-RCP45-70	−3.72	−0.89	4.58	11.57	18.16	23.06	25.93	25.51	21.04	13.66	5.22	−1.83
4-RCP85-50	−4.04	−1.49	4.09	11.02	17.33	22.24	25.40	25.04	20.44	13.19	4.97	−1.92
4-RCP85-70	−1.20	1.45	6.59	12.98	19.02	23.83	26.86	26.49	22.15	15.10	6.91	0.44

Table 12. Climate projections of Tmax for 2031–2050s and 2051–2070s in the two RCP scenarios under the four GCM models in Tanggu.

	Jan	Feb	Mar	Apr	May	Jun	Jul	Aug	Sep	Oct	Nov	Dec
1-RCP45-50	1.91	5	11.31	18.67	25.75	29.83	31.42	30.90	26.79	19.92	11.03	4.08
1-RCP45-70	2.99	5.98	12.37	19.68	26.39	30.29	32.01	31.72	27.61	20.68	11.97	5.20
1-RCP85-50	2.25	4.97	11.37	18.86	25.97	30.51	32.38	31.50	27.12	20.23	11.49	4.71
1-RCP85-70	4.09	7.05	13.40	20.86	27.86	32.04	33.73	33.13	29.14	22.31	13.32	6.32
2-RCP45-50	2.79	5.01	11.53	19.12	25.80	29.53	31.26	31.32	27.59	21.06	12.50	5.74
2-RCP45-70	3.21	5.40	12.11	20.11	27.18	31.48	33.53	33.02	28.96	22.64	13.94	6.55
2-RCP85-50	2.98	5.53	11.76	19.36	26.18	30.32	31.74	31.12	27.40	21.13	12.75	5.88
2-RCP85-70	4.02	6.42	12.84	20.25	27.14	31.44	33.63	33.69	29.90	23.30	14.35	7.07
3-RCP45-50	1.69	4.50	10.98	18.45	25.46	29.41	30.90	30.52	26.58	19.78	11.17	4.32
3-RCP45-70	2.22	5.02	11.42	18.97	25.93	29.71	31.35	31.19	27.25	20.43	11.69	4.73
3-RCP85-50	1.94	4.55	10.97	18.76	25.99	29.70	31.00	30.67	26.98	20.32	11.60	4.63
3-RCP85-70	3.10	5.72	12.11	19.73	26.74	30.61	32.23	32.10	28.35	21.52	12.72	5.74
4-RCP45-50	2.79	5.67	12.47	20.15	27.08	30.76	32.16	31.92	27.95	20.76	11.77	5.13
4-RCP45-70	4.83	8.24	14.37	21.31	28.30	31.81	32.53	32.10	28.52	21.54	12.90	6.66
4-RCP85-50	2.94	6.14	12.95	20.41	27.10	30.81	32.35	32.04	28	20.94	12.10	5.31
4-RCP85-70	5.81	9.03	15.4	22.19	28.59	32.40	33.73	33.47	29.87	22.73	13.77	7.63

3.2. SVM

3.2.1. SVM Operation

SVM is a two-class classifier. Its basic idea is to map data to a high-dimensional space so that the separable data becomes more linearly separable and then find a hyperplane to classify the data. This hyperplane is determined by the support vectors, which are those points closest to the separating hyperplane. The core of the SVM method is to maximize the classification interval in order to find the optimal hyperplane so that the distance between positive and negative samples is maximized.

In this study, an SVM optimization code was written using Python language. The SVM method is used to optimize the data from 2010 to 2020 simulated by LARS-WG, and the optimized R^2 and RMSE are shown in Table 13.

Table 13. Calibration after SVM optimization.

Station	T	R^2	RMSE
Baodi	Tmin	0.868	2.917
	Tmax	0.877	2.66
Tianjin	Tmin	0.871	2.68
	Tmax	0.889	2.56
Tanggu	Tmin	0.893	2.47
	Tmax	0.903	2.36

It can be seen from Table 13 that the R^2 of the lowest 2m-temperature has increased to 0.87–0.89 and the R^2 of the highest 2m-temperature has increased to 0.88–0.90 and the Tmax is better simulated than the Tmin. The simulation accuracy of the Tanggu district is the highest followed by the Tianjin district and the Baodi district.

3.2.2. Future Climate Optimization Based on SVM

It can be seen from Tables 7–12 that the results of the three areas simulated by ACCESS1-3 are almost at the average level of the simulation results of the four models, and the climate differences of Baodi, Tianjin, and Tanggu are not obvious. Therefore, taking the Baodi district as an example, based on the SVM algorithm, the Tmin and Tmax under two scenarios of RCP4.5 and RCP8.5 of 2031–2050s and 2051–2070s in ACCESS1-3 mode are optimized. It can be seen from Figure 4 that the orange line represents the SVR optimization value and the blue line represents the LARS-WG simulation value, and the optimized Tmax, and 2m-temperature in the two scenarios of different ages are basically consistent with the original simulation values. However, in terms of the maximum and minimum values of the optimized 2m-temperature, its value is smaller and the minimum value is larger. Under the RCP4.5 and RCP8.5 scenarios, extreme low 2m-temperatures are more likely to occur around 2036, 2040, 2044, 2048, 2056, 2060, 2064 and 2068, and the lowest 2m-temperature reached −20 °C. After SVR optimization, the span between 2m-temperatures becomes smaller; the lowest 2m-temperature is about −10 °C, and the extreme low 2m-temperature is more likely to occur in 2048 and 2069. From the Tmax of different scenarios, the extreme high 2m-temperature will occur in 2061 and, 2062 in the RCP4.5 scenario; the 2m-temperature is as high as 40 °C. On the whole, the accuracy of the Tmax simulated by SVR optimization is higher than that of the Tmin. Surprisingly, in the RCP8.5 scenario, the optimized and simulated values of Tmax for 2051–2070 are very close to each other, but the Tmax is around 30 °C. These values are repeatedly verified and give the same results. This question will be the direction of the next research.

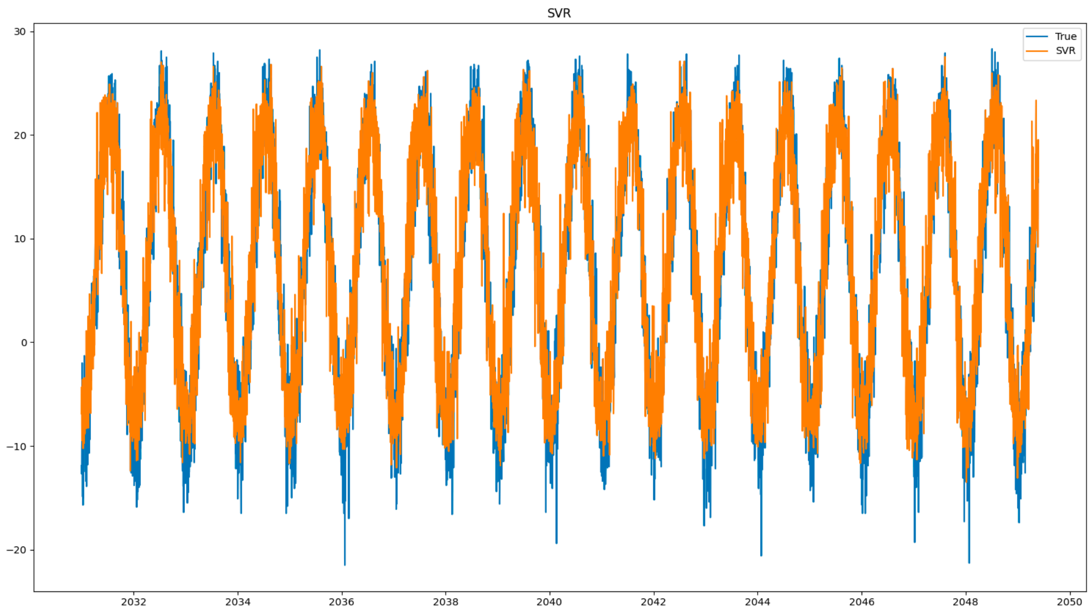

RCP4.5—50Tmin

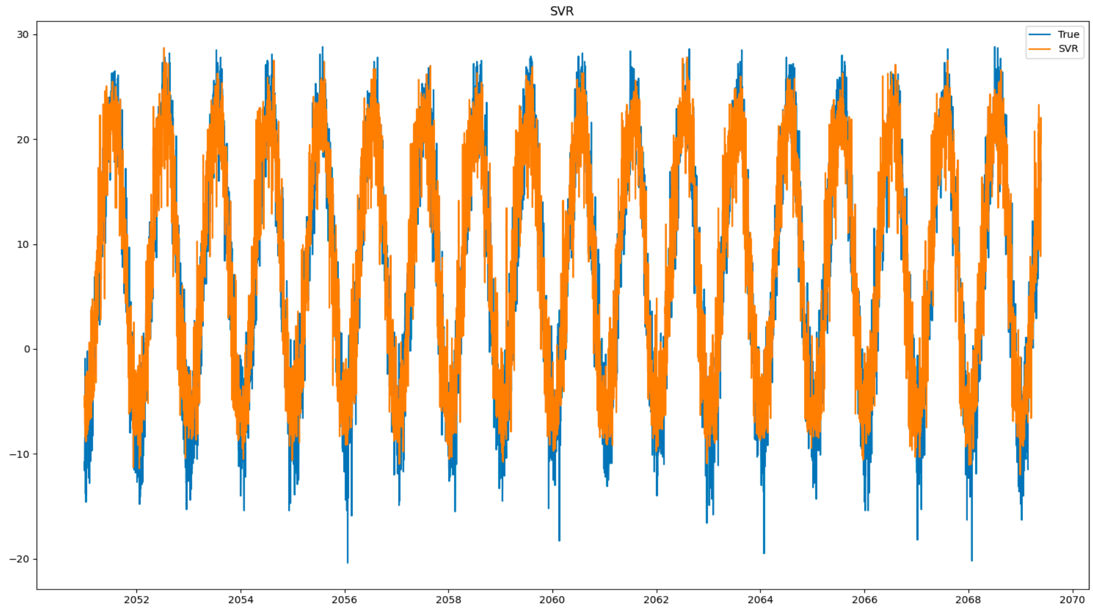

RCP4.5—70Tmin

Figure 4. *Cont.*

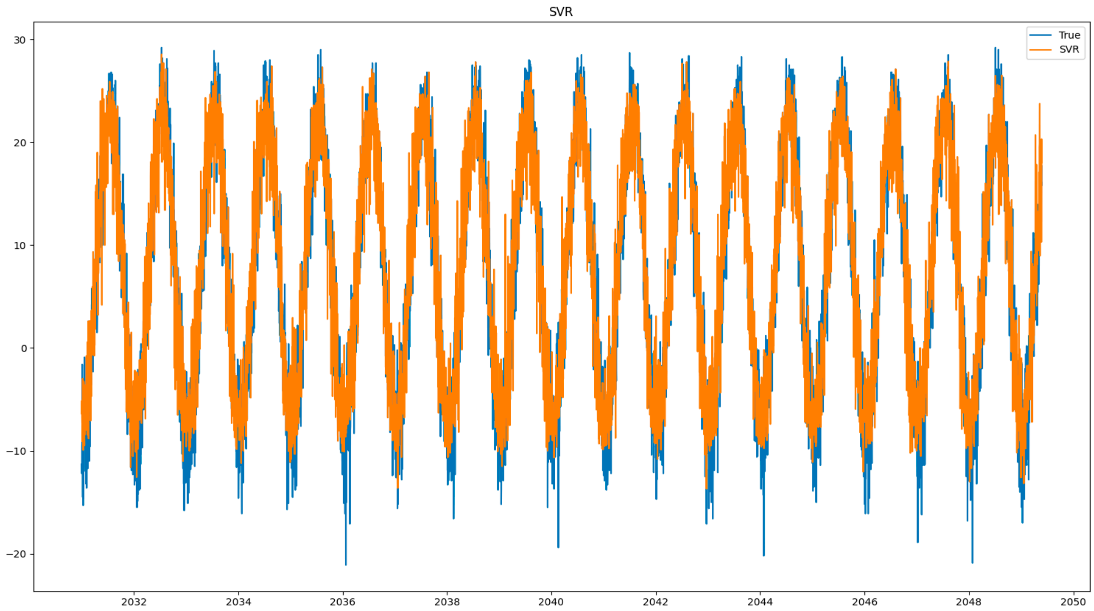

RCP8.5—50Tmin

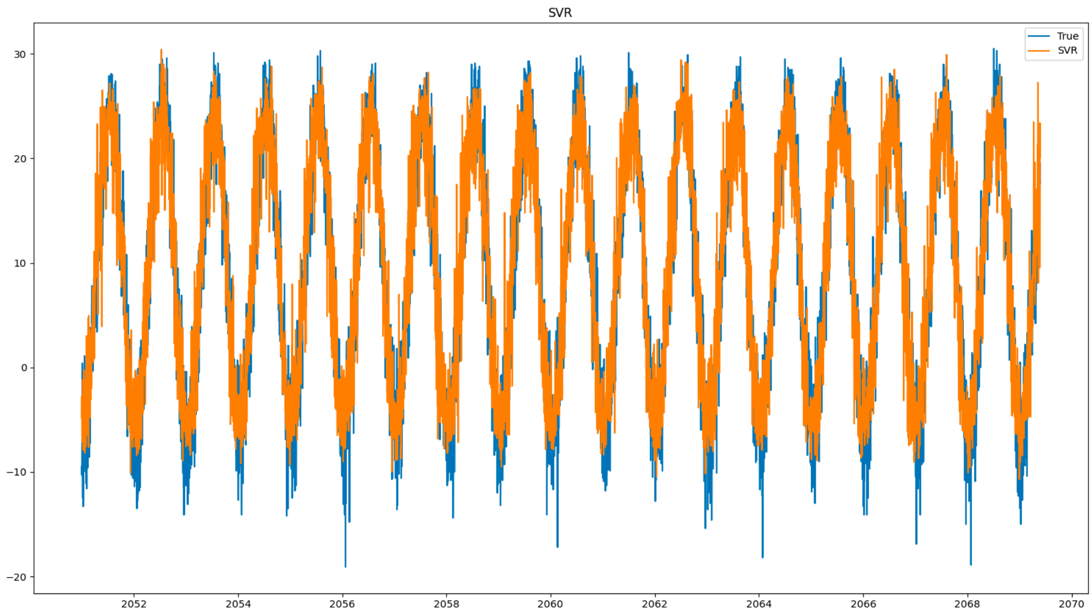

RCP8.5—70Tmin

Figure 4. *Cont.*

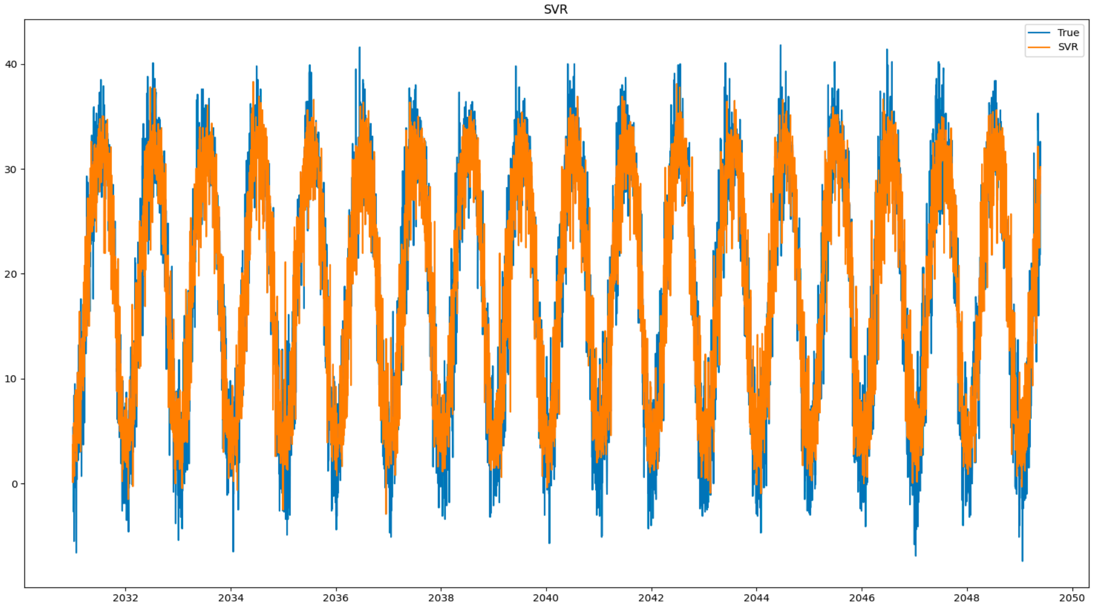

RCP4.5—50Tmax

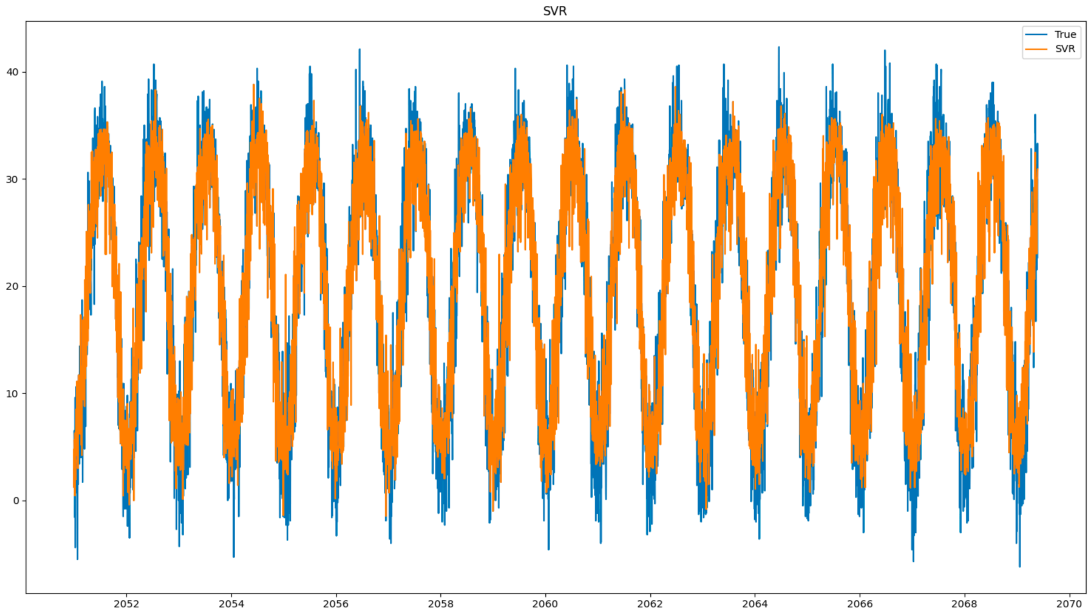

RCP4.5—70Tmax

Figure 4. *Cont.*

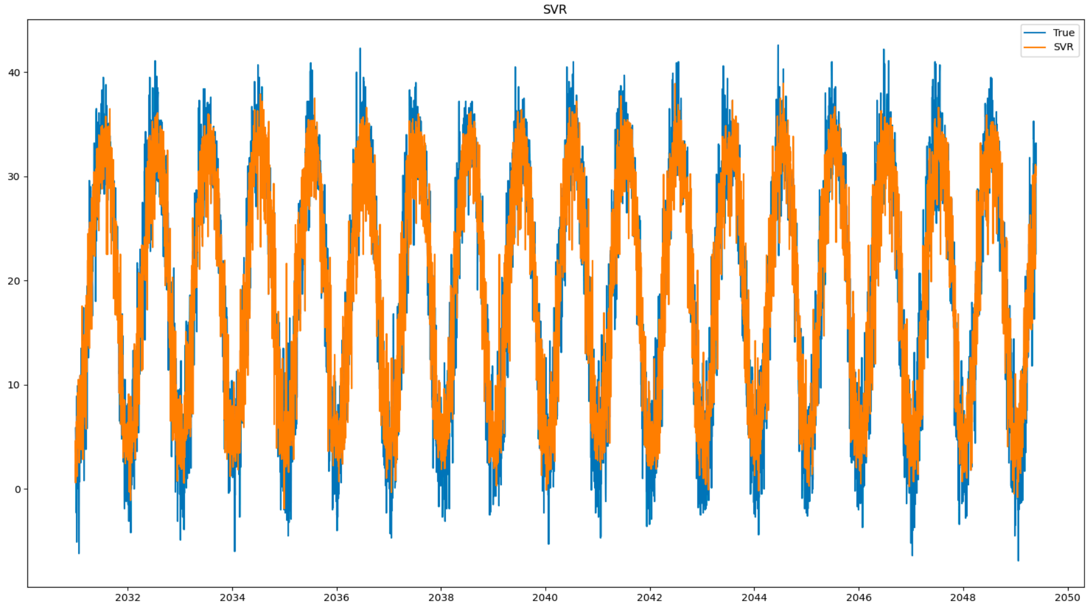

RCP8.5—50Tmax

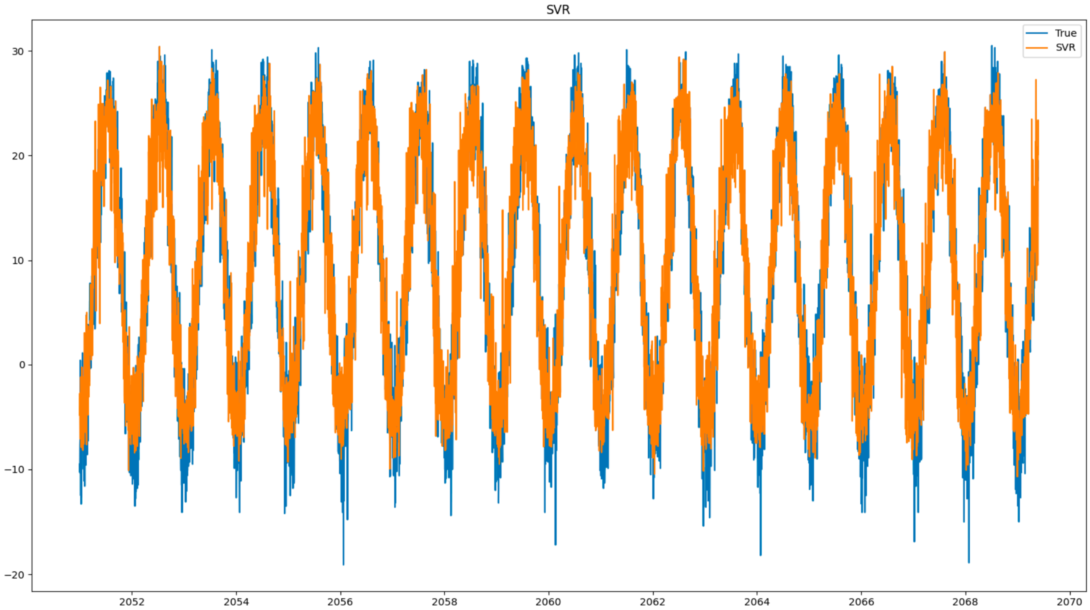

RCP8.5—70Tmax

Figure 4. Future climate optimized by SVM under different scenarios. RCP4.5 represents the RCP4.5 scenario and RCP8.5 represents the RCP8.5 scenario; 50 means 2031–2050s and 70 means 2051–2070s. Note: RCP4.5 represents the RCP4.5 scenario, and RCP8.5 represents the RCP8.5 scenario; 50 means 2031–2050sand 70 means 2051–2070s; Tmin denotes the lowest 2m-temperature and Tmax the highest 2m-temperature.

4. Limitations and Outlooks

This study conducted future climate prediction under the CMIP5 climate model, but compared to the CMIP6 climate model implemented in 2022, the prediction accuracy is slightly lower. In addition, this study only predicted the highest and lowest 2m-temperatures of future weather, without predicting future daily precipitation.

Predicting future climate change is crucial for predicting extreme weather, adjusting crop planting times, increasing pollination rates, and ultimately, increasing yields. Therefore, the focus of future research is to use big data, algorithm models, etc, to conduct big data analysis on the massive data generated by all walks of life under the future climate change.

5. Conclusions

In this study, LARS-WG was used to simulate the maximum, moderate, and Tmin in the future, 2031–2050s and 2051–2070s, under two scenarios of RCP4.5 and RCP8.5 under eight atmospheric circulation models. The SVM is used to optimize the generated future climate data and the predicted future climate is better simulated.

(1) The Tmax R^2 of the LARS-WG simulation is 0.8, and the Tmin R^2 is 0.86–0.87. The Tmin in Tianjin is better simulated by LARS-WG. LARS-WG simulates thefuture climate in EC-EARTH in Tianjin.

(2) LARS-WG simulates the future climate of Tianjin. the Tmin and Tmax in the future simulated by the EC-EARTH model is relatively low, and the Tmin and Tmax simulated by the Had-GEM2-ES4 model is relatively high, especially in the RCP8.5 scenario, where the Tmin and Tmax in the future simulated in the 1970s is the highest.

(3) After SVM optimization, the R^2 of the lowest 2m-temperature is increased to 0.87–0.89, and the R^2 of the highest 2m-temperature is increased to 0.88–0.90, and the Tmax is better simulated than the Tmin. It indicates that the SVM optimization method is suitable for future climate prediction in Tianjin.

(4) The Tmin and Tmax after SVM optimization are basically consistent with the original simulation value, but in terms of the maximum value and minimum value of the Tmin and Tmax optimization, the maximum value after optimization is smaller and the minimum value is larger. This is also a problem that needs to be focused on in future research.

Author Contributions: Conceptualization, Y.W.; data curation, Y.W.; formal analysis, Y.Y.; funding acquisition, Y.W. and X.W.; investigation, W.L.; methodology, Y.W.; project administration, X.W.; resources, Y.W. and Y.Y.; software, Y.W.; supervision, X.L. and W.L.; validation, X.L. and W.L.; visualization, Y.W.; writing—original draft preparation, Y.W.; writing—review and editing, Y.W. and W.L. All authors have read and agreed to the published version of the manuscript.

Funding: This research was funded by [the Cernet Innovation Project] grant number [NGII20190624] and The APC was funded by [the Cernet Innovation Project].

Institutional Review Board Statement: Not applicable.

Informed Consent Statement: Not applicable.

Data Availability Statement: Not applicable.

Acknowledgments: All individuals included in this section have consented to the acknowledgement. We acknowledge the critical comments from anonymous reviewers and editor.

Conflicts of Interest: The authors declare that they have no conflict of interest.

References

1. Sun, W.; Li, Q.; Huang, B.; Cheng, J.; Song, Z.; Li, H.; Dong, W.; Zhai, P.; Jones, P. The Assessment of Global Surface Temperature Change from 1850s: The C-LSAT 2.0 Ensemble and the CMST-Interim Datasets. *Adv. Atmos. Sci.* **2021**, *38*, 875–888. [CrossRef]
2. IPCC. *Climate Change 2013: The Physical Science Basis. Contribution of Working Group I to the Fifth Assessment Report of the Intergovernmental Panel on Climate Change*; Intergovernmental panel on climate Change, working group I contribution to the IPCC fifth assessment report (AR5); Stocker, T.F., Qin, D., Plattner, G.-K., Tignor, M., Allen, S.K., Boschung, J., Nauels, A., Xia, Y., Bex, V., Midgley, P.M., Eds.; Cambridge University Press: New York, NY, USA, 2013; p. 1535.
3. Anderson, T.R.; Hawkins, E.; Jones, P.D. CO_2, the greenhouse effect and global warming: From the pioneering work of Arrhenius and Callendar to today's earth system models. *Endeavour* **2016**, *40*, 178–187. [CrossRef] [PubMed]
4. Saddique, N.; Bernhofer, C.; Kronenberg, R.; Usman, M. Downscaling of CMIP5 models output by using statistical models in a data scarce mountain environment (Mangla Dam Watershed), Northern Pakistan. *Asia-Pac. J. Atmos. Sci.* **2019**, *55*, 719–735. [CrossRef]
5. Wang, J.; Liu, Y.; Ding, Y.; Wu, P.; Zhu, Z.; Xu, Y.; Qi, L. Impacts of climate anomalies on the interannual and interdecadal variability of autumn and winter haze in North China: A review. *Int. J. Climatol.* **2020**, *40*, 4309–4325. [CrossRef]
6. Semenov, M.; Shewry, P. Modelling predicts that heat stress and not drought will limit wheat yield in Europe. *Nat. Preced.* **2010**. [CrossRef]

7. Zhang, J.; Yang, X.H.; Li, Y.Q. A refined rank set pair analysis model based on wavelet analysis for predicting temperature series. *Int. J. Numer. Methods Heat Fluid Flow* **2015**, *25*, 974–985. [CrossRef]
8. Taylor, K.E.; Stouffer, R.J.; Meehl, G.A. An overview of CMIP5 and the experiment design. *Bull. Am. Meteorol. Soc.* **2012**, *93*, 485–498. [CrossRef]
9. Wilks, D.S. Multisite downscaling of daily precipitation with a stochastic weather generator. *Clim. Res.* **1999**, *11*, 125–136. [CrossRef]
10. Semenov, M.A.; Brooks, R.J.; Barrow, E.M.; Richardson, C.W. Comparison of the WGEN and LARS-WG stochastic weather generators for diverse climates. *Clim. Res.* **1998**, *10*, 95–107. [CrossRef]
11. Charles, B.C.; Elijah, P.; Vernon, R.N.C. Climate change impact on maize (*Zea mays* L.) yield using crop simulation and statistical downscaling models: A review. *Sci. Res. Essays* **2017**, *12*, 167–187. [CrossRef]
12. Moghadam, S.H.; Ashofteh, P.S.; Loáiciga, H.A. Investigating the performance of data mining, lumped, and distributed models in runoff projected under climate change. *J. Hydrol.* **2023**, *617*, 128992. [CrossRef]
13. Ahmadi, M.; Etedali, H.R.; Elbeltagi, A. Evaluation of the effect of climate change on maize water footprint under RCPs scenarios in Qazvin plain, Iran. *Agric. Water Manag.* **2021**, *254*, 106969. [CrossRef]
14. Seifi, A.J.; Baghanam, A.H.; Asadi, E.; Hassanzadeh, Y.; Sheikhbabaei, A. Assessing the impact of climate change by using LARS-WG, Case Study Zarineh-rud River Basin. In Proceedings of the 3rd Iranian National Conference on Hydrology, Tabriz, Iran, 17–19 September 2019.
15. Dixit, P.N.; Telleria, R. Advancing the climate data driven crop-modeling studies in the dry areas of Northern Syria and Lebanon: An important first step for assessing impact of future climate. *Sci. Total Environ.* **2015**, *511*, 562–575. [CrossRef]
16. Wang, H.; Wang, L.; Yan, G.; Bai, H.; Zhao, Y.; Ju, M.; Chen, L. Assessment and Prediction of Extreme Temperature Indices in the North China Plain by CMIP6 Climate Model. *Appl. Sci.* **2022**, *12*, 7201. [CrossRef]
17. Gos, M.; Krzyszczak, J.; Baranowski, P.; Murat, M.; Malinowska, I. Combined TBATS and SVM model of minimum and maximum air temperatures applied to wheat yield prediction at different locations in Europe. *Agric. For. Meteorol.* **2020**, *281*, 107827. [CrossRef]
18. Alam, M.S.; Barbour, S.L.; Huang, M.; Li, Y. Using statistical and dynamical downscaling to assess climate change impacts on mine reclamation cover water balances. *Mine Water Environ.* **2020**, *39*, 699–715. [CrossRef]
19. Šípek, V.; Daňhelka, J. Modification of input datasets for the ensemble streamflow prediction based on large-scale climatic indices and weather generator. *J. Hydrol.* **2015**, *528*, 720–733. [CrossRef]
20. Ripendra, A.; Haimanote, B.; Ali, F. Analysis of potential future climate and climate extremes in the brazos headwaters basin, texas. *Water* **2016**, *8*, 603.
21. Roshani, A.; Hamidi, M. Groundwater level fluctuations in coastal aquifer: Using artificial neural networks to predict the impacts of climatical cmip6 scenarios. *Water Resour. Manag.* **2022**, *36*, 3981–4001. [CrossRef]
22. Safavi, H.R.; Sajjadi, S.M.; Raghibi, V. Assessment of climate change impacts on climate variables using probabilistic ensemble modeling and trend analysis. *Theor. Appl. Climatol.* **2017**, *130*, 635–653. [CrossRef]
23. Yoosefdoost, I.; Khasheisiuki, A.; Tabari, H.; Mohammadrezapour, O.; Tsakiris, G. Runoff simulation under future climate change conditions: Performance comparison of data-mining algorithms and conceptual models. *Water Resour. Manag.* **2022**, *36*, 1191–1215. [CrossRef]
24. Cortes, C. Support-Vector Networks. *Mach. Learn.* **1995**, *20*, 273–297. [CrossRef]
25. Kim, Y.; Hong, S. Very Short-term prediction of weather radar-based rainfall distribution and intensity over the Korean Peninsula using convolutional long short-term memory network. *Asia-Pac. J. Atmos. Sci.* **2022**, *58*, 489–506. [CrossRef]
26. Smith, D.M.; Scaife, A.A.; Hawkins, E.; Bilbao, R.; Boer, G.J.; Caian, M.; Yeager, S. Predicted chance that global warming will temporarily exceed 1.5 °C. *Geo. Res. Let.* **2018**, *45*, 11–895. [CrossRef]
27. Tong, S.; Ebi, K. Preventing and mitigating health risks of climate change. *Environ. Res.* **2019**, *174*, 9–13. [CrossRef]
28. Entao, Y. A warmer, wetter and less windy China in the twenty-first century as projected by a nested high-resolution simulation using the Weather Research and Forecasting (WRF) Model. *Asia-Pac. J. Atmos. Sci.* **2019**, *55*, 53–74. [CrossRef]